Active Brownian Particles

Smruti Manjunath

July 5, 2019

Institute for Computational Physics, University of Stuttgart

1 Introduction

An entire class of biological and physical systems which may be referred to as active matter has been studied theoretically and experimentally. There are numerous realizations of self-propelled particles in nature ranging from bacteria and spermatozoa to artificial colloidal microswimmers. The term "active" refers here to the ability of individual units to move actively by gaining kinetic energy from the environment and are statistically described by systems far from equilibrium. An important feature of such systems are the non-negligible random fluctuations in the motion of individual active units. A simple way to account for such fluctuations without being able to resolve the underlying mechanisms is to introduce stochastic forces into the equations of motion of individual particles. Thus our general modelling approach will be based on the concept of stochastic differential equations (Langevin equation).

A major driving force of the active matter research is the realization of active granular and colloidal systems. An analysis of simple dynamical models of active systems is reviewed here. We define active motion as motion of particles or agents due to an internal driving, which may have different causes such as biological activity or non-equilibrium dynamics in artificial driven systems. In particular, we will focus on the mathematical description and analysis of such systems from the purview of Statistical physics.

Here, an experiment demonstrating the sensing of light gradients in synthetic systems, akin to many microorganisms like zooplankton and phytoplankton displaying phototactic behaviour is studied.

2 Experiment:Phototaxis of synthetic microswimmers in optical landscapes

The experiment is performed with photo-activated Janus particles composed of optically transparent silica spheres which are capped on one side with a thin light-absorbing carbon layer. When illumniated, these particles perform a self-diffusiophoretic active motion, with the cap pointing opposite to the direction of motion. The propulsion velocity of the particles is determined by the incident light intensity I, as can be seen from figure 1. The agreement between the data for different intensity gradients demonstrates that v_p is only determined by the local intensity incident on the particle.

When a diluted suspension of microswimmers is subjected to a one dimensional linear intensity gradient ∇I, directed particle motion towards low intensities is observed within a few seconds (Figure 2) . Optical gradient forces can be ruled out as the origin of the observed drift motion. After the light field is turned on at time t_0, particles rotate until their orientation $\hat{u}$ points antiparallel to the gradient. Since $\hat{\mathbf{u}}$ is parallel to the self-propulsion velocity, this results in motion opposite

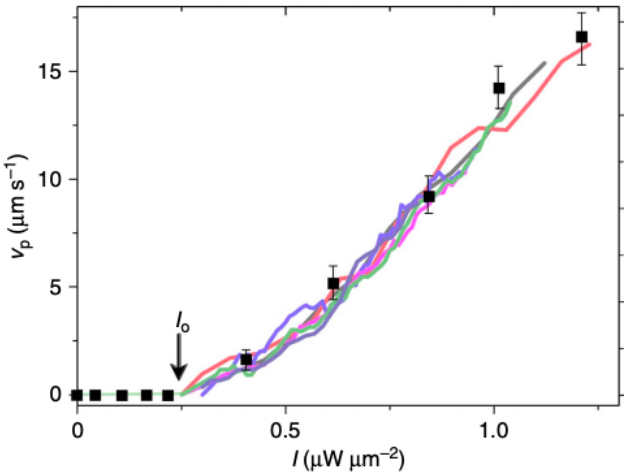

Figure 1: Propulsion velocity v_p versus illumination intensity I. Symbols correspond to homogeneous illumination, with error bars representing standard deviation. Coloured lined correspond to light profiles of different gradients. [1]

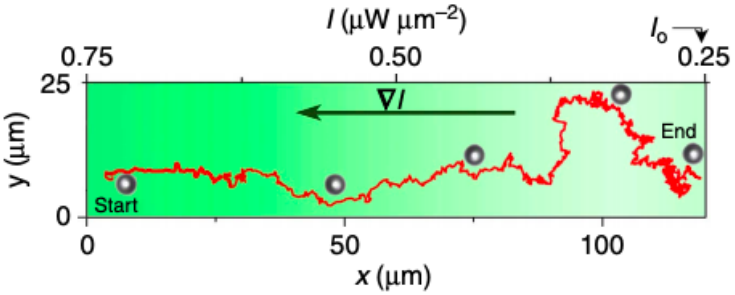

Figure 2: Trajectory of an active particle in an intensity gradient. [1]

to ∇I. The reorientation is caused by breaking the axial symmetry of the slip velocity around the particle because of the inhomogeneous illumination, which leads to a viscous torque acting on the particle. The viscous torque M responsible for particle alignment is proportional to $\nabla I \times \hat{\mathbf{u}}$, so the noise-free angular velocity can be written as

$$\dot{\theta} = \omega_{\max} \sin\theta \tag{1}$$

Here, the amplitude $\omega_{\max}$ sets the time needed to reorient the particle. Since the torque M is expected to depend both on the gradient and the absolute intensity at the particle's position, the gradients of the intensity profiles were varied at different intensities (figure 3).

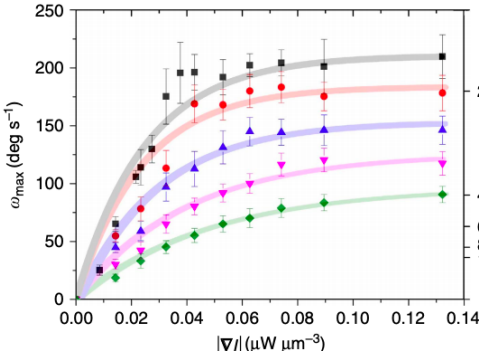

Figure 3: Maximum angular velocity vs intensity gradient for different local densities [1]

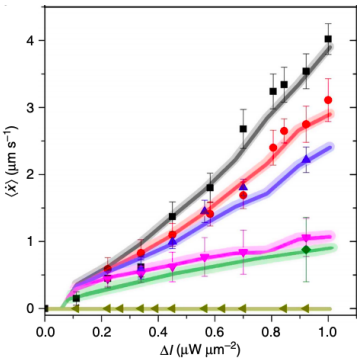

Figure 4: Average velocity vs intensity amplitude. Solid symbols represent experimental data and solid curves represent numerical simulations. [1]

In order to understand the results above, numerical simulations were performed with propulsion velocity and aligning torque. The theoretical model is based on the Langevin equations for the

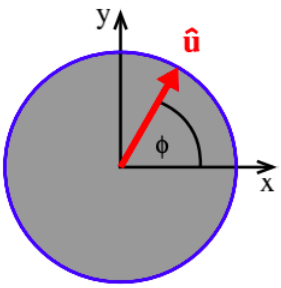

Figure 5: Sketch of a spherical particle with one orientational degree of freedom [2]

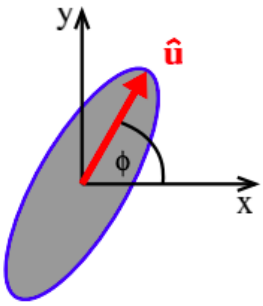

Figure 6: Sketch of Ellipsoidal particle with one orientational degree of freedom[2]

centre-of-mass position $\mathbf{r}(t)$ and the orientation $\hat{\mathbf{u}}(t)$ of the particle:

$$\dot{\mathbf{r}} = v_{\mathrm{p}}(x)\hat{\mathbf{u}} + \zeta_{\mathbf{r}} \tag{2}$$

$$\gamma_{\mathrm{rot}}\dot{\hat{\mathbf{u}}} = (\mathbf{M} + \zeta_{\hat{\mathbf{u}}}) \times \hat{\mathbf{u}} \tag{3}$$

where ζ_r and $\zeta_{\hat{u}}$ are the translational and rotational noise terms respectively. γ_{rot} is the rotational damping constant and sets the scale of the torque M such that γ_{rot}/M gives the reorientation time.

Figure 4 shows that the numerical results, based on a simple model governed by equations 2 and 3 are in good agreement with the experimental data (The error bars correspond to 95% of the confidence interval.), as well as correctly describe the dependence of the average velocity on the intensity amplitude.

In the next section, a comprehensive model of the Langevin dynamics introduced in equations 2 and 3 is presented. Various model situations are considered in increasing order of generality, finally concluding with a suitable model including an aligning torque, to explain the phototactic response observed in microswimmers, above.

3 Brownian motion of a self propelled particle

The framework for theoretical modelling of self-propellers is given by the Langevin theory of a particle with translational and orientational diffusion including an effective internal force in the overdamped Brownian dynamics. So, the model consists of an isotropic or anisotropic self propelled particle which undergoes overdamped Brownian motion and whose propulsion mechanism is described by an effective internal force $\mathbf{F} = F\hat{\mathbf{u}}$, which is included in the Langevin equation.This theoretically assumed internal propulsion force fluctuates in direction as per Brownian motion. $\hat{\mathbf{u}}$, the orientation vector, specifies the direction of self propulsion.

Since a probability distribution can be specified by its moments, which provide an alternative description of the distribution without having to explicitly obtain it, the first four moments are analytically calculated for the model situations considered below.

3.1 A spherical particle with one orientational degree of freedom

The sketch of such a model situation is shown in figure 5. It is useful for describing the motion of a self propelled particle on a substrate. This system consists of a spherical particle whose rotational motion is constrained to a two-dimensional plane. This can be experimentally achieved by externally applied optical fields.

The two dimensional motion of this particle is described by the centre of mass position vector $\mathbf{r}(t) = (x, y)$ and the angle ϕ between $\hat{\mathbf{e}}_{\mathbf{x}}$ and $\hat{\mathbf{u}} = (\cos\phi, \sin\phi)$. Hence, the Langevin equations are given by:

$$\frac{\mathrm{d}\mathbf{r}}{\mathrm{d}t} = \beta D_{\mathrm{t}}[F\hat{\mathbf{u}} - \nabla U + \mathbf{f}] \tag{4}$$

and

$$\frac{\mathrm{d}\phi}{\mathrm{d}t} = \beta D_{\mathrm{r}}\mathbf{g} \cdot \hat{\mathrm{e}}_{\mathrm{z}} \tag{5}$$

$\mathbf{f}(t)$ and $\mathbf{g}(t)$ are the Gaussian white noise random force and torque, respectively, and are characterized by:

$$\langle f_i(t)\rangle = 0, \quad \langle f_i(t) f_j\left(t'\right)\rangle = 2\delta_{ij}\delta\left(t - t'\right) / \left(\beta^2 D_t\right)$$

,

$$\langle g_i(t)\rangle = 0 \quad \langle g_i(t) g_j\left(t'\right)\rangle = 2\delta_{ij}\delta\left(t - t'\right) / \left(\beta^2 D_{\mathrm{r}}\right)$$

The averages are noise-averages, δ_{ij} is the Kronecker delta, for i and j being the corresponding components, and $U(\mathbf{r})$ is the external potential. D_t and D_{r} are the short time translational and rotational diffusion constants, which share the following relationship for spherical particles: $D_{\mathrm{t}}/D_{\mathrm{r}} = 4R^2/3$.

If the initial time is set to be zero, the solutions of the Langevin equations 4 and 5 are given by:

$$\phi(t) = \beta D_{\mathrm{r}} \int_0^t g\left(t'\right) \mathrm{d}t' + \phi_0 \tag{6}$$

and

$$x(t) = \beta D \left[F_0 \int_0^t \cos\phi\left(t'\right) \mathrm{d}t' + \int_0^t f\left(t'\right) \mathrm{d}t' \right] + x_0 \tag{7}$$

where $\phi_0 \equiv \phi\left(t_0\right)$ and $x_0 \equiv x\left(t_0\right)$. Solving equation 5 and averaging, we get:

$$\langle\phi(t)\rangle = \phi_0 \quad \text{and} \quad \left\langle\left(\phi(t) - \phi_0\right)^2\right\rangle = 2D_{\mathrm{r}}t$$

As $\phi(t)$ is a linear combination of Gaussian variables $g\left(t'\right)$, according to Wick's theorem, $\phi(t)$is Gaussian as well. Thus the probability distribution of ϕ is:

$$P(\phi, t) = \frac{1}{\sqrt{4\pi D_{\mathrm{r}}t}} \exp\left(-\frac{\left(\phi - \phi_0\right)^2}{4D_{\mathrm{r}}t}\right) \tag{8}$$

Since only the projected force $F_0 \cos\phi$ drives the particle, the mean particle position is calculated from:

$$\langle\cos\phi(t)\rangle = \int_{-\infty}^{\infty} \cos(\phi) P(\phi, t) \mathrm{d}\phi = e^{-D_{\mathrm{r}}t} \cos\phi_0 \tag{9}$$

which gives (inserting ratio of $D_{\mathrm{t}}/D_{\mathrm{r}}$):

$$\langle x(t) - x_0\rangle = \frac{4}{3}\beta F_0 R^2 \cos\left(\phi_0\right)\left[1 - e^{-D_x t}\right] \tag{10}$$

. For short times, this approximates to:

$$\langle x(t) - x_0\rangle = \frac{4}{3}\beta F_0 R^2 \cos\left(\phi_0\right) D_{\mathrm{r}}t + \mathcal{O}\left(t^2\right) \tag{11}$$

and for $t \gg D_{\mathrm{r}}^{-1}$ the ϕ_0 -dependent mean position converges towards

$$\lim_{t\to\infty} \langle x(t) - x_0\rangle = \frac{4}{3}\beta F_0 R^2 \cos\left(\phi_0\right) \tag{12}$$

To calculate the mean square displacement, the following integrals have to be solved:

$$\left\langle (x(t)-x_0)^2 \right\rangle = \beta^2 D^2 \left[F_0^2 \int_0^t \mathrm{d}t_1 \int_0^t \mathrm{d}t_2 \left\langle \cos\phi\left(t_1\right)\cos\phi\left(t_2\right)\right\rangle \right. \tag{13}$$
$$\left. +2F_0 \int_0^t \mathrm{d}t_1 \int_0^t \mathrm{d}t_2 \left\langle \cos\phi\left(t_1\right) f\left(t_2\right)\right\rangle + \int_0^t \mathrm{d}t_1 \int_0^t \mathrm{d}t_2 \left\langle f\left(t_1\right) f\left(t_2\right)\right\rangle \right]$$

The third summand is easily calculated to be $2t/\left(\beta^2 D\right)$. The second summand vanishes as $\langle\cos\phi(t)\rangle$ only depends on $g(t)$, so $\langle\cos\phi(t)\rangle$ and $f(t)$ are statistically independent. The first summand is calculated using a time correlation function (see [3], for details).The mean square displacement thus takes the final form:

$$\left\langle (x(t)-x_0)^2 \right\rangle = 2D_t t + \left(\frac{4}{3}\beta F_0 R^2\right)^2 \left[e^{-D_x t} + D_\mathrm{r} t - 1 + \frac{1}{12}\cos\left(2\phi_0\right)\left(e^{-4D_\mathrm{r} t} - 4e^{-D_\mathrm{r} t} + 3\right)\right] \tag{14}$$

The long-time diffusion coefficient D_1 is given by:

$$D_1 = \lim_{t\to\infty} \frac{1}{2t}\left\langle (x(t)-x_0)^2 \right\rangle = D_t + \frac{8}{9}\left(\beta F_0 R^2\right)^2 D_\mathrm{r} \tag{15}$$

To investigate the non-Gaussian behaviour of the particle, the Skewness S and Kurtosis γ are calculated as follows:

$$S = \frac{\langle (x-\langle x\rangle)^3\rangle}{\langle (x-\langle x\rangle)^2\rangle^{3/2}} \quad \gamma = \frac{\langle (x-\langle x\rangle)^4\rangle}{\langle (x-\langle x\rangle)^2\rangle^2} - 3 \tag{16}$$

The third and fourth moments are calculated by solving the following integrals, in analogy with the method used to calculate mean square displacement, including time correlation functions:

$$\begin{aligned}\left\langle (x(t)-x_0)^3 \right\rangle =& \beta^3 D^3 \int_0^t \mathrm{d}t_1 \int_0^t \mathrm{d}t_2 \int_0^t \mathrm{d}t_3 \left[F_0^3 \cos\phi\left(t_1\right)\cos\phi\left(t_2\right)\cos\phi\left(t_3\right)\right\rangle \\ &+ 3F_0 \left\langle\cos\phi\left(t_1\right)\right\rangle \left\langle f\left(t_2\right) f\left(t_3\right)\right\rangle]\end{aligned} \tag{17}$$

and

$$\begin{aligned}\left\langle (x(t)-x_0)^4 \right\rangle =& \beta^4 D^4 \int_0^t \mathrm{d}t_1 \int_0^t \mathrm{d}t_2 \int_0^t \mathrm{d}t_3 \int_0^t \mathrm{d}t_4 \left[F_0^4 \left\langle\cos\phi\left(t_1\right)\cos\phi\left(t_2\right)\cos\phi\left(t_3\right)\cos\phi\left(t_4\right)\right\rangle \right. \\ &\left. + 6F_0^2 \left\langle\cos\phi\left(t_1\right)\cos\phi\left(t_2\right)\right\rangle \left\langle f\left(t_3\right) f\left(t_4\right)\right\rangle + \left\langle f\left(t_1\right) f\left(t_2\right) f\left(t_3\right) f\left(t_4\right)\right\rangle\right]\end{aligned} \tag{18}$$

The particle motion can be characterized qualitatively into three different time regimes (Figure 7). At short and long time scales, the behaviour is diffusive whereas at intermediate timescales, the mean square displacement shows a t^3 dependence. At early times $t \ll t_1$, the particle undergoes simple translational Brownian motion, governed by the short-term diffusion term $(8/3)R^2 D_\mathrm{r} t$. The multiplicative coupling of a diffusive and a ballistic behaviour for the angular and the translational displacements, respectively, is what leads to $\left\langle (x(t)-x_0)^2 \right\rangle \propto t^3$ [2]. This regime is terminated by the timescale t_2 beyond which it is diffusive again, as governed by equation (15).

It is also interesting to analyse the Kurtosis, which gives the leading long-time behaviour as:

$$\gamma(t) = \frac{-21F_s^{*4}}{9 + 12F_s^{*2} + 4F_s^{*4}}\left(D_\mathrm{r} t\right)^{-1} + \mathcal{O}\left(\frac{1}{t^2}\right) \tag{19}$$

Figure 8 shows deviation from zero in the kurtosis, which depicts crossover to non-Gaussian behaviour. The long-time tail indicates that the behaviour of the particle is still non-Gaussian when its motion is diffusive again.

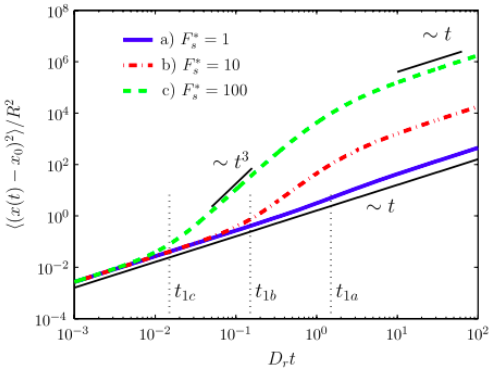

Figure 7: Mean-square displacement of a spherical particle for different values of $F_s^* = \beta R F$ [2]

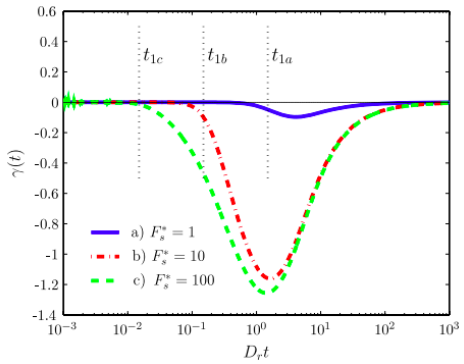

Figure 8: Kurtosis of the probability distribution function [2]

Next, we briefly consider the model with translation along a plane. The analytical expressions for the first and second moments based on the two-dimensional Langevin equation (4) are given by a superposition of the motion in the x and y directions. We thus obtain a vectorial mean position:

$$\langle \mathbf{r}(t) - \mathbf{r}_0 \rangle = \frac{4}{3} \beta F R^2 \left[1 - \mathrm{e}^{-D_r t} \right] \begin{pmatrix} \cos(\phi_0) \\ \sin(\phi_0) \end{pmatrix} \tag{20}$$

and mean square displacement:

$$\left\langle (\mathbf{r}(t) - \mathbf{r}_0)^2 \right\rangle = \frac{16}{3} R^2 D_\mathrm{r} t + 2 \left(\frac{4}{3} \beta F R^2 \right)^2 \left[D_\mathrm{r} t - 1 + \mathrm{e}^{-D_\varepsilon t} \right] \tag{21}$$

Due to free translational motion in the 2D plane, the ϕ_0 dependence vanishes. It can also be seen that the diffusive term here is twice as large as equation (14).

3.2 Ellipsoidal particle with one orientational degree of freedom

This situation is depicted in figure 6. Here, the translational diffusion coefficient is anisotropic, so the diffusion tensor is applied. $\hat{\mathbf{u}} = (\cos\phi, \sin\phi)$; D_a and D_b indicate the diffusion coefficients for translation in the direction of the two semi-axes of the ellipsoid. Thus, the Langevin equation, including the diffusion tensor becomes:

$$\frac{\mathrm{d}\mathbf{r}}{\mathrm{d}t} = \beta \mathbf{D}_\mathrm{t} \cdot [F \hat{\mathbf{u}} - \nabla U] + \mathbf{w} \tag{22}$$

with a zero mean random noise source $\mathbf{w}(t)$. The variances are given by: $\langle w_i(t) w_j(t') \rangle = 2 D_t^{ij}(\phi(t)) \delta(t - t')$

Since $\mathbf{D_t} \cdot \hat{\mathbf{u}} = D_a \hat{\mathbf{u}}$, the 1D Langevin equation becomes:

$$\frac{\mathrm{d}x}{\mathrm{d}t} = \beta D_a F \cos(\phi) + w_x \tag{23}$$

The mean square displacement is given by:

$$\begin{aligned} \left\langle (x(t) - x_0)^2 \right\rangle &= 2\overline{D} t + \tfrac{\Delta D}{4 D_\mathrm{r}} \cos(2\phi_0) \left(1 - \mathrm{e}^{-4 D_t t} \right) \\ &+ \left(\beta F \tfrac{D_a}{D_\mathrm{r}} \right)^2 \left[D_\mathrm{r} t - 1 + \mathrm{e}^{-D_t t} \right. \\ &\left. + \tfrac{1}{12} \cos(2\phi_0) \left(3 - 4\mathrm{e}^{-D_t t} + \mathrm{e}^{-4 D_t t} \right) \right] \end{aligned} \tag{24}$$

where $\Delta d = D_a - D_b$. The ϕ_0 dependence is observed very early, from the second term, which is still in the regime of bare translational diffusion. The additional term represents the relative orientation of the initial direction of the long axis of the ellipsoidal particle and the direction of the linear channel.

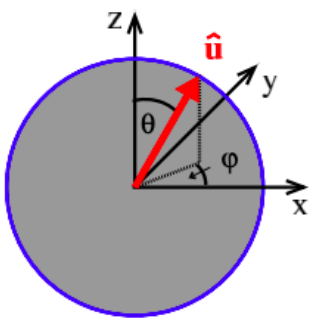

Figure 9: Sketch of freely rotating spherical particle [2]

3.3 Freely rotating spherical particle

This model includes particles whose orientation is freely diffusing on the unit sphere. The orientation angle is now given by $\hat{\mathbf{u}} = (\sin\theta\cos\varphi, \sin\theta\sin\varphi, \cos\theta)$ in terms of two orientation angles (figure 9). The same Langevin equation for the centre of mass position as in equation 4 can be considered here, with the third component of all vectorial quantities considered additionally.

The orientational probability distribution for the freely diffusing orientation vector is given by the spherical harmonics:

$$P(\theta,\varphi,t) = \sum_{l=0}^{\infty}\sum_{m=-l}^{l} \mathrm{e}^{-D_\mathrm{r} l(l+1)t} Y_l^{m*}(\theta_0,\varphi_0)\, Y_l^m(\theta,\varphi) \tag{25}$$

In the case of choosing the linear channel along the z direction, the first moment is obtained as:

$$\langle z(t) - z_0\rangle = \frac{2}{3}\beta F R^2 \cos(\theta_0)\left(1 - \mathrm{e}^{-2D_\mathrm{t}t}\right) \tag{26}$$

This is very similar to equation (10) where the azimuthal angle θ takes the role of ϕ_0 in (10), and the two results agree up to linear order in time t. The mean square displacement is obtained from equation 25:

$$\begin{aligned}\left\langle (z(t)-z_0)^2\right\rangle &= \tfrac{8}{3}R^2 D_\mathrm{r} t + \left(\tfrac{2}{9}\beta F R^2\right)^2 \\ &\times \Big[12 D_\mathrm{r} t - 8 + 9\mathrm{e}^{-2D_\mathrm{r}t} - \mathrm{e}^{-6D_\mathrm{r}t} \\ &+ \cos^2(\theta_0)\left(6 - 9\mathrm{e}^{-2D_\mathrm{t}t} + 3\mathrm{e}^{-6D_\mathrm{r}t}\right)\Big]\end{aligned} \tag{27}$$

Upon comparing with that for 1 orientational degree of freedom, it can be seen that the mean square displacements are almost identical. The crossover timescale t_1 is thus identical and t_2 is half as large for the former case. Thus, here, the long-time diffusion constant is smaller:

$$D_\mathrm{L} = \frac{4}{3} D_\mathrm{r} R^2 \left[1 + \frac{2}{9}(\beta R F)^2\right] \tag{28}$$

The negative $1/t$ long-time t tail in kurtosis is present even for the present model, so it can be inferred that it is unaffected by the number of orientational degrees of freedom (figure 10).

The analytical results obtained thus far can be used to compare with experimental systems of, for example, swimming bacteria or self-propelled colloidal particles. Any deviations point to the importance of hydrodynamic interactions with the substrate. It is important to note that hydrodynamic interactions were neglected so far, which may significantly influence the mean square displacement's distributions. A non-Gaussian noise might also be relevant for modelling real swimming objects.

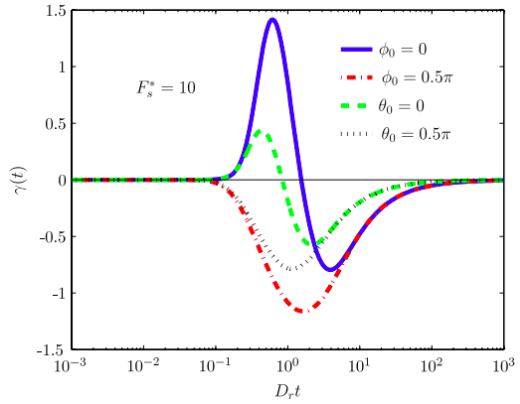

Figure 10: Kurtosis of spherical particle for one (blue, red) and two (green, black) orientational degrees of freedom[2]

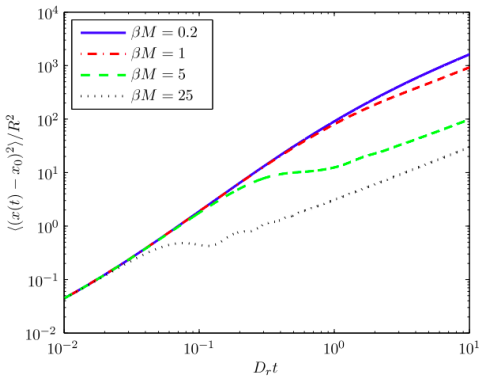

Figure 11: Mean square displacement of a spherical particle with additional external torque [3]

3.4 Presence of additional torque

To address the model discussed in the experiment in section 2, in addition to the intensity-dependent particle velocity, a torque M due to the light gradient must be taken into account. The noise terms in equations (2) and (3) are defined by the variances $\langle \zeta_{\mathbf{r}}(t_1) \otimes \zeta_{\mathbf{r}}(t_2) \rangle = 2D_{\mathrm{tr}} \not\Vdash \delta(t_1 - t_2)$ and $\langle \zeta_\varphi(t_1)\, \zeta_\varphi(t_2) \rangle = 2D_{\mathrm{rot}} \delta(t_1 - t_2)$. Following the notation introduced in section 3, the Langevin equation for the orientational angle ϕ would be given by:

$$\frac{\mathrm{d}\phi}{\mathrm{d}t} = \beta D_{\mathrm{r}}[M + g(t)] \tag{29}$$

Solving this, we obtain:

$$\langle \phi(t) \rangle = \phi_0 + \beta D_{\mathrm{r}} M t = \phi_0 + \omega t \tag{30}$$

with frequency $\omega = \beta D_{\mathrm{r}} M$ and $\langle (\phi(t) - \langle \phi(t) \rangle)^2 \rangle = 2D_{\mathrm{r}} t$. Replacing the ϕ_0 in the probability distribution (8) with $\phi_0 + \omega t$ and then calculating the mean position, we get:

$$\begin{aligned} \langle x(t) - x_0 \rangle =& \frac{\beta D}{(D_{\mathrm{r}}^2 + \omega^2)} F_0 \left[D_{\mathrm{r}} \cos(\phi_0) - \omega \sin(\phi_0) \right. \\ & \left. + e^{-D_{\mathrm{r}} t} \left(\omega \sin(\phi_0 + \omega t) - D_{\mathrm{r}} \cos(\phi_0 + \omega t) \right) \right] \end{aligned} \tag{31}$$

The long-time diffusion coefficient is given by:

$$D_1 = D + \frac{8}{9} \frac{(\beta F_0 R^2)^2 D_{\mathrm{r}}}{(1 + (\beta M)^2)} \tag{32}$$

The mean square displacement for such a model is sketched in figure 11. If the torque is a time-dependent torque, i.e, $M(t)$, then the mean square displacement takes the form:

$$\begin{aligned} \left\langle (x(t) - x_0)^2 \right\rangle =& 2Dt + \beta^2 F_0^2 D^2 \int_0^t \mathrm{d}t_1 \int_0^{t_1} \mathrm{d}t_2 e^{-D_x (t_1 - t_2)} \\ & \times \left[\cos(\omega_{t_1} - \omega_{t_2}) + \cos(2\phi_0 + \omega_{t_1} + \omega_{t_2})\, e^{-4D_t t_2} \right] \end{aligned} \tag{33}$$

4 Active Brownian particles and Run-and-Tumble particles

Active Brownian particles (ABP) swim at fixed speed v along a body-axis u that rotates by slow angular diffusion. Run-and-tumble particles (RTP), like motile bacteria, swim with constant u

until a random tumble event suddenly changes the orientation. One class of self-propelled colloids is represented by motile bacteria such as E-Coli, which move in a series of runs and tumbles, which occur randomly at a rate α. At large scales, and under conditions of constant v, α, a single RTP performs a random walk with diffusivity $D_0 = v^2/\alpha d$ and cannot be distinguished from passive Brownian particles at equilibrium. However, if their swim speed $v(\rho)$ decreases fast enough with local particle density ρ RTPs undergo phase separation between a dense, slow-swimming fluid and a dilute fast-swimming one. Another class, represented by synthetic (bi-)metallised colloids create a self-phoretic local chemical motor by catalysing the breakdown of hydrogen peroxide. Their swimming direction changes gradually, by rotational diffusion. This rotation is usually Brownian in origin. At time scales large compared to the angular reorientation time τ ($\sim 1/D_r$ or $\sim 1/\alpha$), and length scales large compared to $\ell = v\tau$, a leading-order exact equivalence between ABPs and RTPs can be established provided that the motility parameters v, α, D_r are independent of particle orientation. Under these conditions thus, ABPs will generically show the same sort of phase separation, subject to the requirement of a sufficiently decreasing $v(\rho)$. This becomes relevant in the parameter space of many body phenomena, namely, motility-induced bulk phase separation. However, no general equivalence exists for cases involving u-dependent motility parameters, and hydrodynamic interactions, which have been neglected so far can induce subtle differences between them.

5 Bibliography

1. Lozano, C. *et al.* Phototaxis of synthetic microswimmers in optical landscapes. *Nat. Commun.* 7:12828 doi: 10.1038/ncomms12828 (2016)

2. B ten Hagen *et al.* 2011 *J. Phys.: Condens. Matter* **23** 194119

3. B ten Hagen *et al.* 2009 *cond-mat.soft* **12** 725

4. M. E. Cates and J. Tailleur 2013 *EPL* **101** 20010

5. Sven van Teeffelen and Hartmut Löwen 2008 *Phys. Rev. E.* **78** 020101(R)

6. P. Romanczuk *et al.* 2012 *Eur. Phys. J. Special Topics* **202** 1-162

7. Fernando Peruani and Luis G. Morelli 2007 *Phys. Rev. Lett.* **99** 010602

8. *The Langevin Equation* https://www2.ph.ed.ac.uk/ dmarendu/ASP/Section14.pdf

9. M. E. Cates and J. Tailleur 2008 *Phys. Rev. Lett.* **100** 218103

10. Joakim Stenhammar *et al.* 2013 *Phys. Rev. Lett.* **111** 145702

11. *Active Brownian Particles: An interactive tutorial* https://warwick.ac.uk/fac/sci/physics/staff/research/cwhitfield/abpsimulations/

12. B. Lindner and E.M. Nicola 2008 *Eur. Phys. J. Special Topics* **157** 43–52